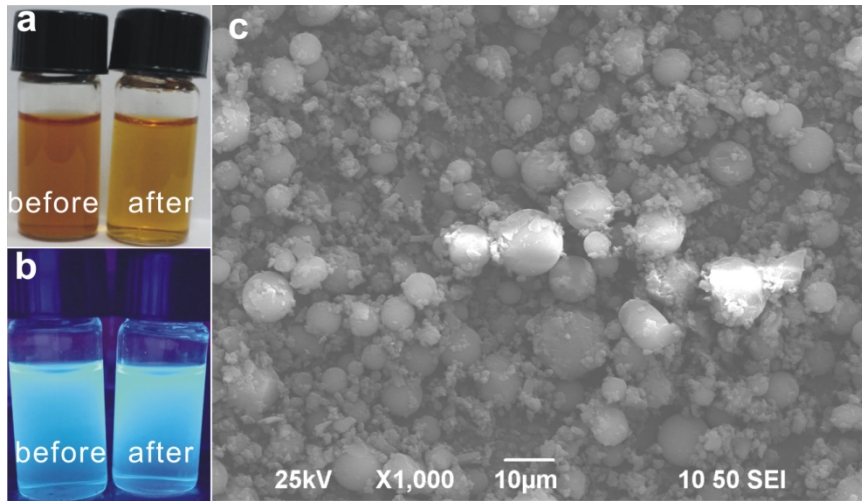


**Fluorescent carbon quantum dots, capacitance and catalysis active porous carbon microspheres  
from beer**

**Zhiyong Gao,<sup>a</sup> Xiaorui Wang,<sup>a</sup> Jiuli Chang,<sup>a</sup> Dapeng Wu,<sup>a</sup> Lan Wang,<sup>a</sup> Xiao Liu,<sup>a</sup> Fang Xu,<sup>a</sup>  
Yuming Guo,<sup>a</sup> Kai Jiang<sup>\*a</sup>**

<sup>a</sup> School of Chemistry and Chemical Engineering, Collaborative Innovation Center of Henan Province for Motive Power & Key Materials, Collaborative Innovation Center of Henan Province for Green Manufacturing of Fine Chemicals, Key Laboratory of Green Chemical Media and Reactions, Ministry of Education, Henan Normal University, Xinxiang, 453007, China.

*E-mail: [kjiang512@163.com](mailto:kjiang512@163.com)*



**Fig. S1** CQDs solution before and after hydrothermal treatment under natural light (a) and UV lamp (b).  
(c) SEM of the formed precipitate.

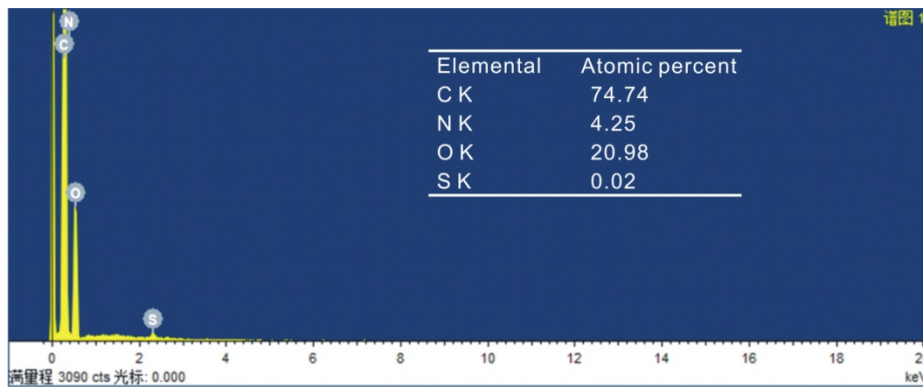


**Fig.S2** EDS of NCQDs.

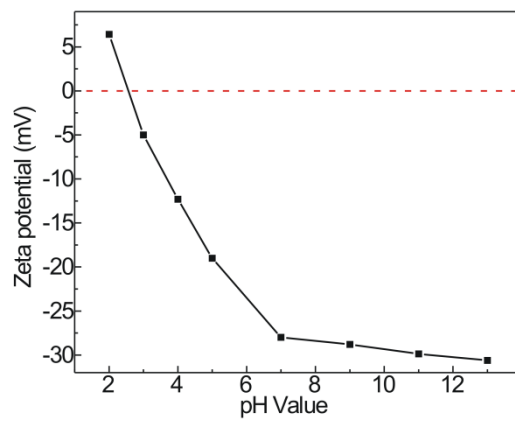


**Fig. S3** Zeta of CQDs aqueous solution at different pH media.

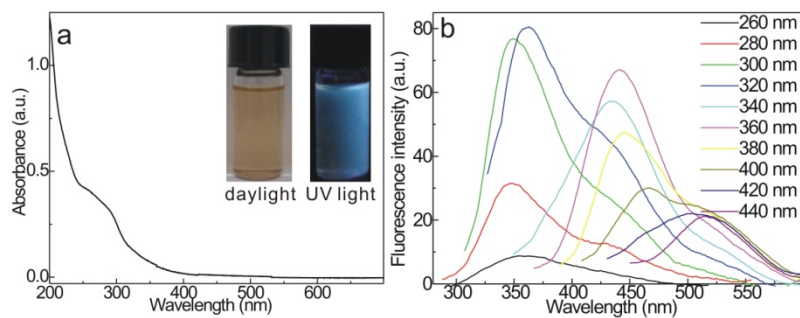


**Fig. S4** (a) UV-vis absorption spectrum and (b) excitation wavelength dependent fluorescence spectra of maltose hydrothermal synthesized carbon quantum dots. Inset in panel a: image of maltose derived carbon quantum dots solution under daylight and UV light.

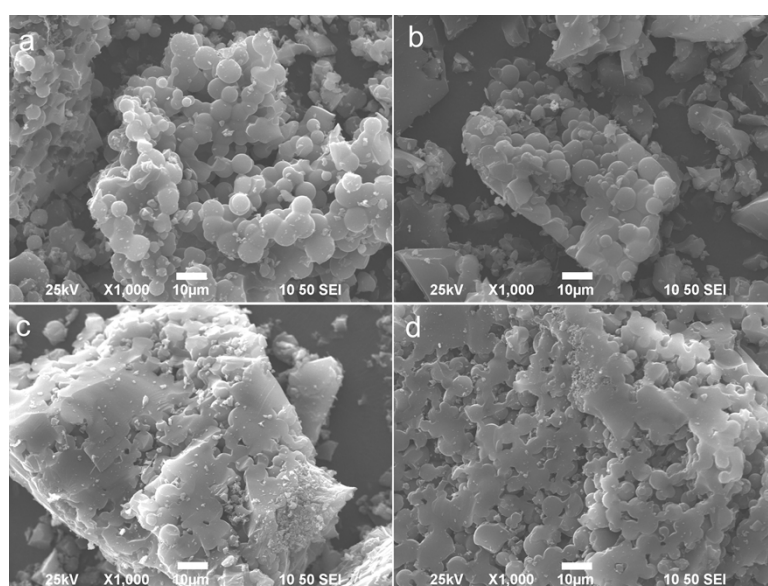


**Fig. S5** SEM of (a) a-PCM<sub>600</sub>, (b) a-PCM<sub>700</sub>, (c) a-PCM<sub>800</sub>, and (d) a-PCM<sub>900</sub>.

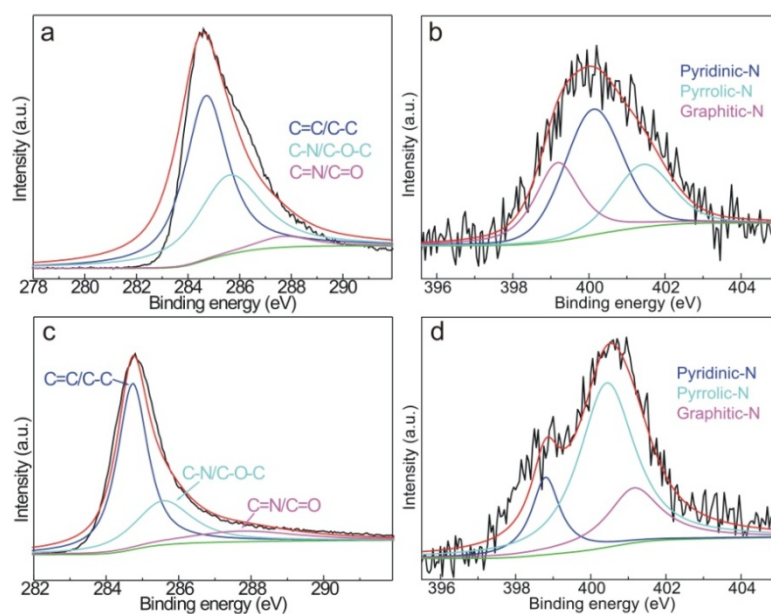


**Fig. S6** High resolution C1s (a, c) and N1s (b, d) XPS spectra of PCM (a, b) and a-PCM<sub>600</sub> (c, d).

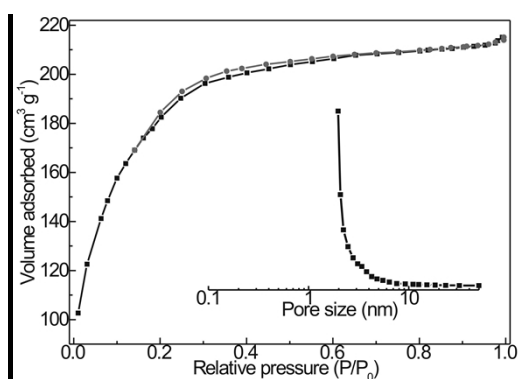


**Fig. S7** N<sub>2</sub> sorption isotherm and BJH pore size distribution of PCM.

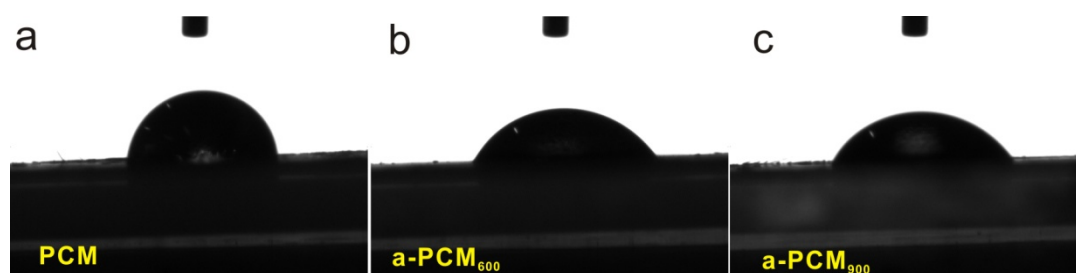


**Fig. S8** Contact angle tests of (a) PCM, (b) a-PCM<sub>600</sub> and (c) a-PCM<sub>900</sub>.

**Table S1** Surface and pore properties of PCM and a-PCMs.

Sample	$S_{\text{BET}}^{\text{a}}$ (m <sup>2</sup> g <sup>-1</sup> )	$S_{\text{micro}}^{\text{b}}$ (m <sup>2</sup> g <sup>-1</sup> )	$S_{\text{meso}}^{\text{c}}$ (m <sup>2</sup> g <sup>-1</sup> )	Pore volume <sup>d</sup> (cm <sup>3</sup> g <sup>-1</sup> )
PCM	488.2	317.6	170.6	0.246
a-PCM <sub>600</sub>	2120.7	1613.0	507.7	1.163
a-PCM <sub>700</sub>	1917.8	1467.3	450.5	1.028
a-PCM <sub>800</sub>	1779.5	1379.4	400.1	0.956
a-PCM <sub>900</sub>	1727.2	1214.6	512.6	0.947

<sup>a</sup> Specific surface area from multiple BET method. <sup>b</sup> Micropore surface area from t-plot method. <sup>c</sup> The t-method external surface area ( $S_{\text{meso}}=S_{\text{BET}}-S_{\text{micro}}$ ). <sup>d</sup> Total pore volume at  $p/p_0=0.99$ .

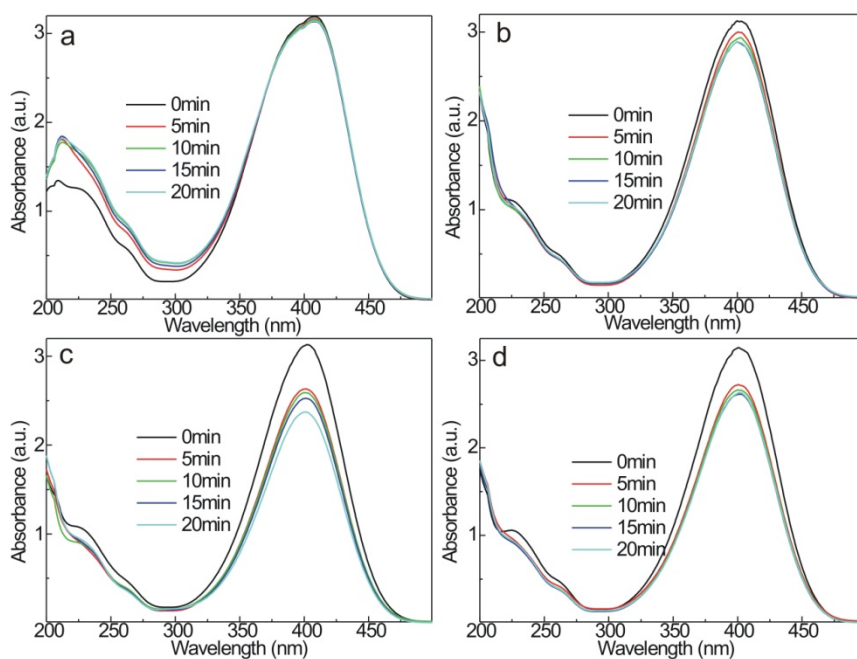


**Fig. S9** UV-vis absorption spectra during the catalytic reduction of 4-nitrophenol by (a) PCM, (b) a-PCM<sub>600</sub>, (c) a-PCM<sub>700</sub> and (d) a-PCM<sub>800</sub>.

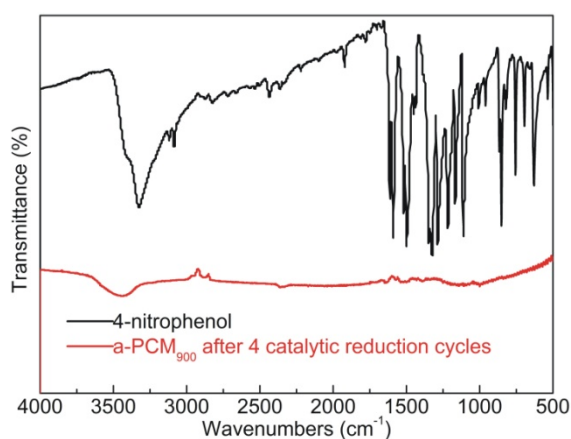


**Fig. S10** FTIR of 4-nitrophenol and the a-PCM<sub>900</sub> catalyst after 4 cycles of catalytic reduction reaction.

From the FTIR spectra, characteristic absorption peaks belonging to 4-nitrophenol can not be observed in the catalyst, which excludes the adsorption of 4-nitrophenol onto catalyst. This result also manifests that decreased UV-Vis absorbance of 4-nitrophenol is caused by the catalytic reduction reaction.